Synchronization of diffusively coupled oscillators near the homoclinic bifurcation

Dmitry Postnov,[1,2] Seung Kee Han,[1] and Hyungtae Kook[3]
[1]*Department of Physics, Chungbuk National University, Cheongju, Chungbuk 361-763, Korea*
[2]*Department of Physics, Saratov State University, Astrakhanskaja st. 83, Saratov 410026, Russia*
[3]*Department of Physics, Kyungwon University, Sungnam, Kyunggi 461-701, Korea*
(Received 5 March 1999)

It has been known that a diffusive coupling between two limit cycle oscillations typically leads to the in-phase synchronization and also that it is the only stable state in the weak-coupling limit. Recently, however, it has been shown that the coupling of the same nature can result in the distinctive dephased synchronization when the limit cycles are close to the homoclinic bifurcation, which often occurs especially for the neuronal oscillators. In this paper we propose a simple physical model using the modified van der Pol equation, which unfolds the generic synchronization behaviors of the latter kind and in which one may readily observe changes in the sychronization behaviors between the distinctive regimes as well. The dephasing mechanism is analyzed both qualitatively and quantitatively in the weak-coupling limit. A general form of coupling is introduced and the synchronization behaviors over a wide range of the coupling parameters are explored to construct the phase diagram using the bifurcation analysis. [S1063-651X(99)02309-0]

PACS number(s): 05.45.−a, 87.10.+e, 82.40.Bj

I. INTRODUCTION

Synchronizations between nonlinear oscillations are abundant in a variety of situations ranging from physical to biological phenomena [1,2]. In particular, recent studies to understand information processings of the nervous systems have been guided by the idea that synchronization of oscillatory neuronal units may provide a mechanism for functioning of the neural systems, which has been supported by experimental observations [3,4]. More specifically, it has been suggested that the temporal correlation scheme among oscillatory neuronal units may underlie the mechanism for the feature binding and segmentation in the sensory perceptions [5].

A prototype of the nonlinear oscillations may be provided by the well-known van der Pol oscillator which was originally devised as a model in the electronic circuit theory [6]. Dynamic behaviors of the oscillator are rather simply predicted from the existence of a single equilibrium (source) and a single limit cycle in the phase space. Often arising in many physical systems with an inherent nonlinear energy dissipation, such a limit cycle oscillation naturally occurs as a balance between the energy generation at a small amplitude oscillation near the source and the energy dissipation at a large amplitude. The coupled dynamics of such oscillations has also been studied extensively and it has been well known from the literatures that a diffusive coupling between two such oscillations typically leads to the in-phase synchronization and also that the in-phase synchronization is the only stable state in the weak-coupling limit [7,8].

Meanwhile, a rather different kind of synchronization behavior has been observed for the coupled neuronal oscillators in a certain range of the oscillator parameters [9,10]. That is, it has been shown that the in-phase synchronization may not be stable for the diffusively coupled neuronal oscillators even when the coupling strength is sufficiently weak. Such examples of neuronal models include the Morris-Lecar [12] and the Hindmarsh-Rose model [13]. Even though these models may exhibit different specifics in detail, their dynamics are qualitatively the same since they share the common structure of phase space that is based on the existence of three equilibria and one limit cycle. The equilibria correspond to a stable node (N), a saddle (S), and an unstable focus (F), respectively. The limit cycle is located at the boundary that limits flows diverging out of the focus. A typical phase portrait is depicted in Fig. 1.

The two coexisting attractors represent the two possible states of a spiking neuron. That is, the stable node corresponds to the resting state and the limit cycle to the sustained firing state of a neuron. The stable manifolds of the saddle separate the phase space into two attraction basins. Consequently, a stimulus to a resting neuron may not lead to firing of the neuron unless it is strong enough to push the trajectory over the separatrix into the other basin for the firing state.

When two neurons are in the firing state and are coupled to each other diffusively, the coupling results in the (phase-locked) synchronization of two oscillations. The phase-locking, however, is not necessarily of in-phase even in the regime of the weak-coupling strength, in contrast to the case of the coupled van der Pol oscillations. Instead, the phase relation between them depends on details of the nature of the oscillations as well as the coupling itself, which will be explained more in the following sections. Preceding studies have pointed out that the instability of the in-phase synchronization is essentially due to the vector field deformation in

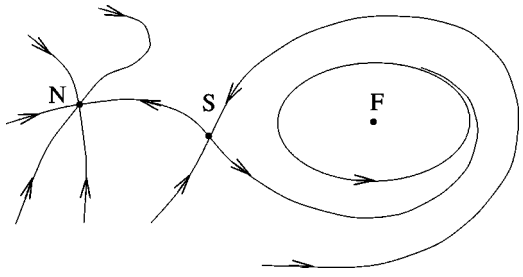

FIG. 1. Typical phase portrait of the neuronal oscillators.

the presence of the saddle point near the limit cycle, which implies the situation when the limit cycle is close to the homoclinic bifurcation [10,11].

In the present study we consider in detail the dephased synchronization not just in the context of the neuronal models but as a generic phenomenon that occurs in coupled oscillators near the homoclinic bifurcation. In doing so, we consider to which class of two-dimensional oscillators the particular neuron models belong. This analysis allows us to propose a transparent model system through a minor modification of the van der Pol oscillator (Sec. II). The proposed model of the coupled oscillators manifests the dephased synchronization as observed in the neuronal models. Furthermore, the variation of parameters can change the properties of the model system from the ''classical'' van der Pol behavior to the neuronal one. This fact also allows us to investigate the dephasing behavior *quantitatively* (Sec. III).

Because the dephasing effect was found strongly dependent on the coupling direction, the introduction of a general vector form of coupling appears to be a natural logical step for our study (Sec. IV). The synchronization behaviors over a wide range of the coupling parameters are explored in Sec. V using the techniques of the bifurcation analysis to construct the phase diagrams. Finally, the results observed from the proposed abstract model are compared with the specific example of the neuronal oscillator model.

II. MODIFIED van der POL OSCILLATOR

A general form of two-dimensional oscillatory systems can be given in the following form:

$$\ddot{x}+F_1(x,\dot{x},\mathbf{p})\dot{x}+F_2(x,\mathbf{p})=0, \tag{1}$$

where the vector $\mathbf{p}$ represents a set of the control parameters. The functions F_1 and F_2 can be given arbitrarily as long as they fulfill conditions for the existence of an oscillation. In the given form F_1 is responsible for the energy dissipation and F_2 for the force exerted on the oscillator. The zeros of F_2 determine the locations of the equilibria, and their stabilities are determined from the signs of dF_2/dx and F_1 at each equilibrium: dF_2/dx is negative only for saddles, and a node and a focus are stable when F_1 is positive.

The simplest example of a nonlinear oscillator of such form is given by the van der Pol oscillator,

$$F_1=\alpha(x^2-1), \quad F_2=x. \tag{2}$$

For positive α the only equilibrium at $x=0$ is an unstable focus since F_1 is negative for $|x|<1$. In addition, since the energy is dissipated at the large distances ($|x|>1$), there also exists a stable limit cycle enclosing the focus with a finite amplitude. Consequently, the global dynamic behavior of the van der Pol oscillator can be predicted from the simple structure of the phase space that contains only one unstable focus and a limit cycle.

The neuronal oscillator models can also be represented in the form of Eq. (1). That is, for the case of the Morris-Lecar model those functions are given as

$$\begin{aligned} F_1(v,\dot{v}) &= \bar{g}_{Ca}\frac{\partial m_\infty(v)}{\partial v}(v-1)+\frac{f}{\tau_w(v)} \\ &\quad +\frac{\bar{g}_{Ca}m_\infty(1-v_k)+\bar{g}_L(v_L-v_K)+I_{\mathrm{dc}}-\dot{v}}{v-v_k}, \\ F_2(v) &= \frac{f}{\tau_w(v)}\{\bar{g}_K(v-v_K)w_\infty(v) \\ &\quad +\bar{g}_{Ca}m_\infty(v)(v-1)+\bar{g}_L(v-v_L)-I_{dc}\}, \end{aligned} \tag{3}$$

where the dimensionless variable v stands for the membrane potential of the neuron and I_{dc} represents the external current input which plays as a main control parameter of the model. More details for the model equation with the notations for the other parameters can be easily found in the literature [10,12].

In the typical regime of the parameters, F_2 has three zeros that correspond to a stable node, a saddle, and an unstable focus, respectively. When the value of I_{dc} is small, the stable node is the only attractor. Then the resulting system becomes excitable; a small stimulus does not induce firings, which corresponds to an insignificant fluctuation of the phase flow near the stable node, whereas a large enough stimulus may lead to a firing of the neuron, which corresponds a long excursion of the flow across the separatrix formed by the stable manifolds of the saddle. Firings are not sustained in the latter case unless stimuli are repeated.

However, as I_{dc} is increased, the homoclinic bifurcation occurs at $I_{\mathrm{dc}}\approx 0.0729$ on which the stable and the unstable manifold of the saddle are connected to form a loop homoclinic to the saddle. Beyond the bifurcation point, a stable limit cycle exists, the flow on which corresponds to the sustained periodic firings. Consequently, in this parameter regime the phase space contains three equilibria together with a limit cyle, as its typical phase portrait can also be given by Fig. 1. This structure of phase space can be readily predicted from the shape of the functions F_1 and F_2 as shown in Fig. 2(a). That is, three equilibria are located at the zeros of F_2 and the type of each equilibrium is determined from the signs of F_1 and dF_2/dx. In the figure, F_1 is given as a contour plot in the $(v,\dot{v})$ plane and the dark area corresponds to the negative dissipation (the energy generation).

As indicated above, the limit cycle oscillations that are close to the homoclinic bifurcation are typical in the neuronal oscillators. Therefore, in understanding systematically the generic behaviors of the coupled dynamics between such oscillations, it would be desirable to have a simple oscillator model that is easily controllable and that still shares the features of interest with the neuronal oscillators as well. For this purpose we propose a simple model as follows and the present study will be focused on the quantitative examinations on this model.

The model is obtained from the van der Pol oscillator, while a slight modification is needed to maintain the required structure of the phase space; hereafter, this model will be called the modified van der Pol (MVP) model. That is, to have three equilibria, we need to introduce a nonlinear cubic force:

$$F_1(x)=\alpha(x^2-\mu),$$

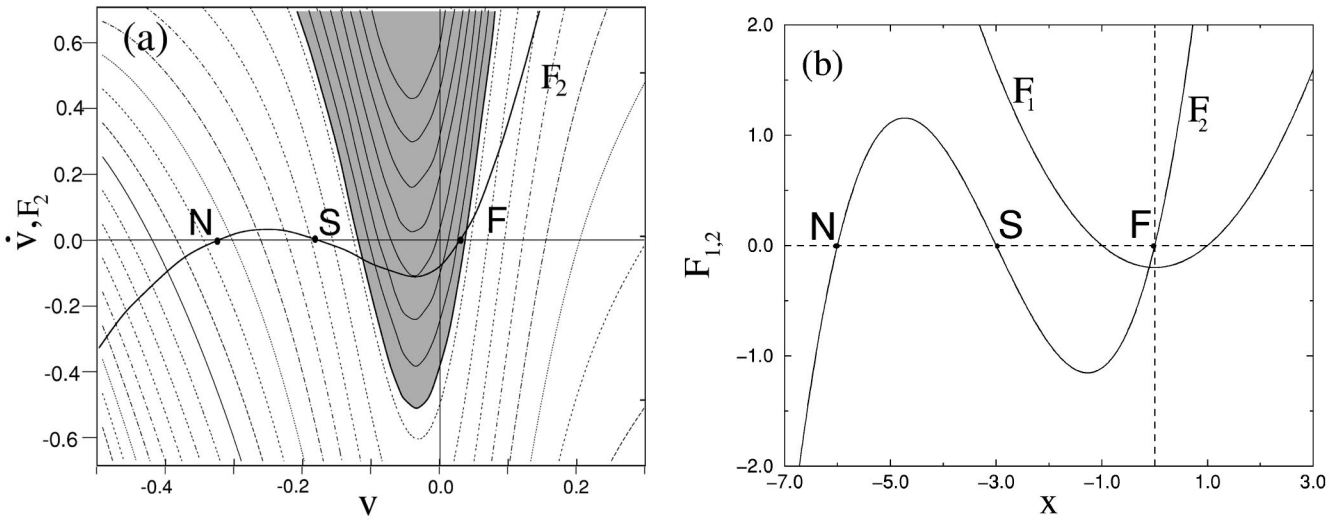

FIG. 2. (a) Function plot of $F_2(v)$ and contour plot of $F_1(v,\dot{v})$ for the Morris-Lecar model. The dark area corresponds to the negative dissipation, i.e., $F_1<0$. (b) Function plots of $F_1(x)$ and $F_2(x)$ for the MVP model.

$$F_2(x)=x(x+d)(x+2d)/d^2, \tag{4}$$

where α, μ, and d are the control parameters that assume positive values.

The MVP model maintains the features of the neuronal models in that the phase space has basically the same structure as shown in Fig. 1. The function plots for F_1 and F_2 are shown in Fig. 2(b). The three equilibrium points are located at $\dot{x}=0$ and $x_{F,S,N}=0,-d,-2d$ for the focus, the saddle, and the stable node, respectively. Also, the slopes of F_2 at the equilibria are $dF_2/dx=2,-1,2$, respectively. The focus is unstable since F_1 is negative at x_F and the limit cycle is located in between the unstable focus and the saddle. In this presentation we set $d=3$ and $\alpha=0.2$. For the fixed values of d and α, the distance to the homoclinic bifurcation is controlled by μ; the limit cycle gets closer to the saddle as μ is increased and the homoclinic connection occurs at $\mu \approx 1.255$. The limit cycle far from the bifurcation with a small μ reduces to the similar situation of the van der Pol oscillation.

In the following sections we will consider various coupling configurations. For this purpose it turns out that a more convenient form for the MVP model is provided by the canonical form of Eq. (1):

$$\begin{aligned}\dot{x}&=y,\\ \dot{y}&=-F_1(x,y)y-F_2(x).\end{aligned} \tag{5}$$

III. DEPHASING OF SYNCHRONIZED OSCILLATIONS NEAR THE SADDLE

In this section, using the coupled MVP model, we consider the synchronization behaviors between two limit cycle oscillations near the homoclinic bifurcation based on the dephasing mechanism of phase flows near the saddle point.

Let us consider a simpler case of the single-variable coupling. That is, the coupled MVP model with a diffusive position-variable coupling is given as

$$\begin{aligned}\dot{x}_1&=y_1+\varepsilon(x_2-x_1),\\ \dot{y}_1&=-F_1y_1-F_2,\end{aligned} \tag{6}$$

where the coupling strength ε is assumed to be sufficiently small so that the perturbation raised in each subsystem is negligibly small. The coupling term for the other oscillator is given symmetrically as $\varepsilon(x_1-x_2)$.

Figure 3 shows the contour plot for the magnitude of the phase velocity v_ϕ for the single oscillator in the absence of coupling; the phase velocity defined as $v_\phi=\sqrt{\dot{x}^2+\dot{y}^2}$ vanishes at the equilibria (S and F). For small μ values, the limit cycle is located far from the saddle. Then the phase space structure in terms of the v_ϕ surface along the limit cycle is qualitatively equivalent to that of the van der Pol oscillator, for which it is known that a diffusive coupling typically leads to the stable in-phase synchronization. An examplary limit cycle trajectory at $\mu=0.2$ is depicted as Γ_1 in the figure.

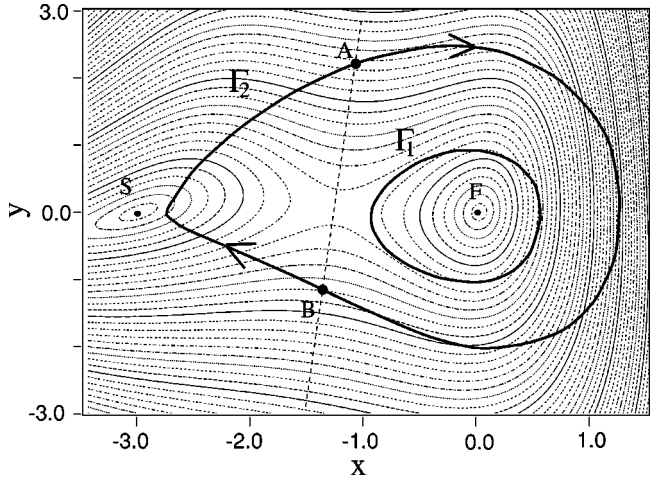

FIG. 3. Contour plot of v_ϕ and location of limit cycles for the MVP model. The limit cycles are drawn for $\mu=0.2$ (Γ_1) and $\mu=1.0$ (Γ_2).

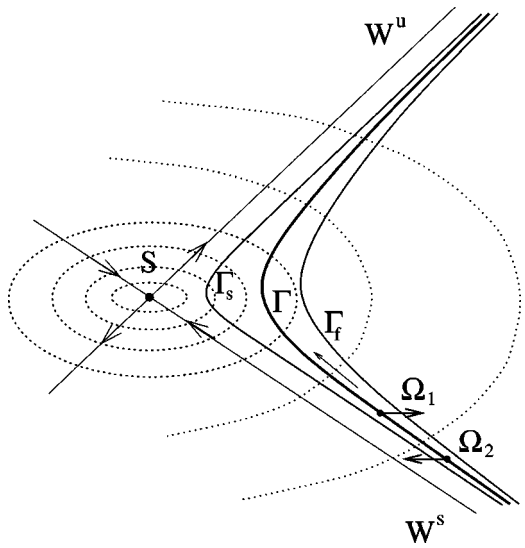

FIG. 4. Phase flows near the saddle (S).

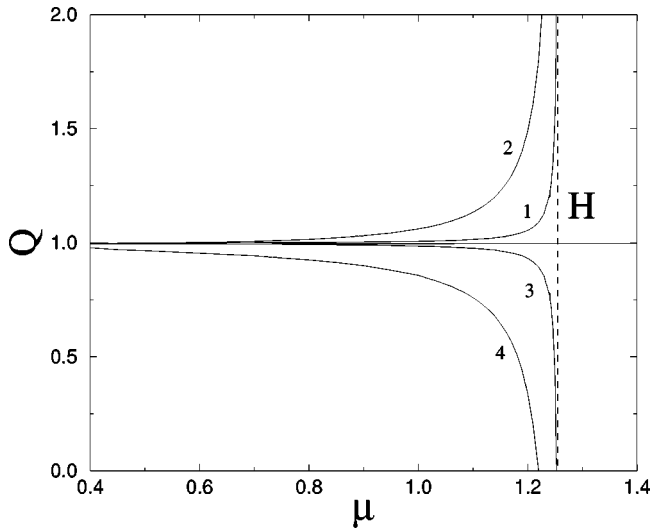

FIG. 5. Q versus μ, the linear dephasing rate. The dotted line H denotes the homoclinic bifurcation point.

However, as μ is increased, the limit cycle gradually approaches close to the saddle and the shape of the v_ϕ surface explored by the limit cycle becomes qualitatively different from the small μ case. The limit cycle trajectory at $\mu=1.0$ is plotted and labeled as Γ_2 in Fig. 3. A trajectory on Γ_2 spends most time near the saddle and, therefore, the interaction due to coupling in this region becomes important. Notice that since v_ϕ together with the vector field changes as μ changes, it is impossible to plot both Γ_1 and Γ_2 in the same plot. Accordingly, in Fig. 3, only Γ_2 has been plotted with numerical accuracy while the plot of Γ_1 has been added only schematically to help compare the two cases.

The flows of the vector field in the vicinity of the saddle and the dephasing behavior in the presence of coupling are depicted schematically in Fig. 4 for the case of the diffusive position coupling as given in Eq. (6). The circles around S represent the v_ϕ contour lines and W^s and W^u represent the stable and the unstable manifolds of the saddle, respectively. Γ denotes the limit cycle trajectory in the absence of coupling and Γ_s and Γ_f denote trajectories of each oscillator perturbed due to coupling, as will be explained further below.

Suppose there is a small time lag between two oscillators when they enter into the vicinity of the saddle. That is, the one oscillator (Ω_1) advances in phase the other (Ω_2) as depicted at the bottom of Γ. Then, the coupling force on Ω_1 acts in the positive x direction where the flow velocity is faster, whereas the coupling force on Ω_2 acts in the other direction where the flow velocity is slower. Therefore, the trajectory of Ω_1 is gradually pushed to the trajectory Γ_f which is faster than Γ and the trajectory of Ω_2 to Γ_s which is slower. As a result, the initial time lag diverges. This implies that the in-phase synchronization can be unstable, which is contrary to the synchronization behavior observed in the coupled van der Pol oscillators.

It should be notified that the dephasing does not necessarily occur all the time when the limit cycle is close to the saddle point. A similar consideration can also be given to show that the diffusive ''velocity-coupling'' leads to the in-phase synchronization; in this case the coupling force would be in the vertical direction in Fig. 4, and hence attractive.

To get a quantitative estimate for the dephasing between the oscillators, let us first divide the limit cycle into two pieces by a line AB as shown in Fig. 3. It is expected that the effect of coupling in the region of the saddle (to the left of AB) is much more relevant to the synchronization. We introduce the measures P and Q for the linear rate of dephasing as follows:

$$\Delta t_B = P\Delta t_A, \qquad \Delta t_A = Q\Delta t_B, \tag{7}$$

where Δt in the right-hand side of Eq. (7) is an initial time lag at the location A or B, and Δt in the left is the evolved time lag measured at the other side. The values of P and Q are to be determined in the limit of the small initial Δt.

The numerical investigations for the coupled MVP model show that P is insensitive to μ ($P\approx 1$). Meanwhile, Q strongly depends on μ. The variation of Q versus μ is shown in Fig. 5 for different coupling strengths and different coupling variables as well. As can been seen in the figure, the position coupling (curves 1 and 2) leads to stronger dephasing as μ approaches the value of the homoclinic bifurcation, $\mu\approx 1.255$. The other case of the velocity coupling (curves 3 and 4) leads to in-phasing. The trend of both in-phasing and dephasing becomes stronger as the coupling strength becomes stronger: compare the curves 2,4 for $\varepsilon=0.01$ with the curves 1,3 for the $\varepsilon=0.001$.

IV. VECTOR COUPLING

For a diffusively coupled system, the coupling term in general would be proportional to both differences x_1-x_2 and y_1-y_2. A simpler case might be conceived in which the coupling is through only a single variable, either the position or the velocity. For instance, as often considered in the studies of the coupled oscillators, only the position coupling can be employed. The examples include the electronic circuits with a purely resistive coupling between component circuits, the inertial coupling for mechanical oscillator systems, and the neuron models with the electric coupling. In more real-

istic circumstances, however, the two-variable coupling seems to be more natural. For instance, the reactance present in electronic circuits or the propagation time delay of the impulses along the neuronal axon may well require couplings between oscillator units through the velocity variable.

In the following we attempt to consider the general case of the two-variable coupling and choose a form called the vector coupling. That is, the coupling is introduced using a vector $\mathbf{K}=(K_x,K_y)$ as follows:

$$\begin{aligned}\dot{x}_1&=y_1+K_x(x_2-x_1),\\ \dot{y}_1&=-F_1y_1-F_2+K_y(y_2-y_1).\end{aligned}\tag{8}$$

For the other oscillator the coupling term is obtained by interchanging x_1 and y_1 with x_2 and y_2, respectively. That is, the coupling is given symmetrically. Such a form of coupling has been previously considered for studies in different contexts [7,8].

In the present work we represent the vector coupling using the polar coordinate:

$$\begin{aligned}K_x&=K\cos\Psi,\\ K_y&=K\sin\Psi.\end{aligned}\tag{9}$$

That is, K denotes the coupling strength and the angle Ψ denotes the relative weight of coupling between two variables. Ψ can also be viewed as the orientation angle of the coupling force in the two-dimensional subspace of each oscillator. As special cases, the coupling force becomes attractive to each other when $\Psi=\pi/4$ and repulsive when $\Psi=5\pi/4$. The single-variable coupling cases are achieved when $\Psi=0,\pi$ (the position-coupling) and $\Psi=\pm\pi/2$ (the velocity-coupling), respectively. The ''purely'' diffusive coupling refers to the regime where neither K_x nor K_y is negative, that is, where $0\leqslant\Psi\leqslant\pi/2$.

V. SYNCHRONIZATION OF THE COUPLED MVP OSCILLATORS

The presentation of the observations on the synchronization behaviors of the coupled MVP equations is divided in three subsections below. The first part considers the case when the coupling strength is sufficiently weak so that an analytic method can be applicable. The second part considers the case of the finite coupling strength and shows how the results in the weak-coupling limit extend in this regime, let alone some additional behaviors. The third part considers the strong-coupling strength regime with an intermediate value of μ where the coupled oscillators are placed in an intermediate distance to the homoclinic bifurcation.

A. Weak-coupling limit

First, we consider the weak-coupling case in which the coupling raises only a negligible perturbation to the limit cycles of the uncoupled oscillators. It is well known that such limits can be analyzed using the phase model reduction method [1,14]. That is, in this scheme, each limit cycle is approximated with the uncoupled one and the phase dynamics between oscillators due to coupling can be analyzed merely from the antisymmetric part, $\Gamma_a^{\rm eff}(\Delta\phi)$, of the *effective coupling function*, $\Gamma^{\rm eff}(\Delta\phi)$, defined as

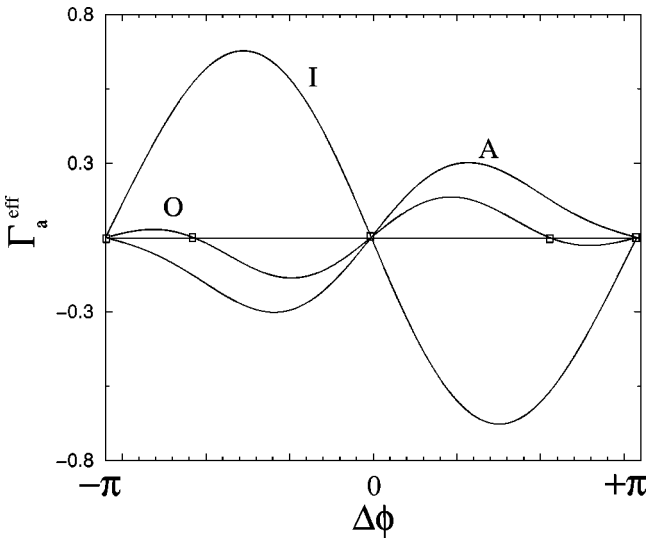

FIG. 6. Plots of $\Gamma_a^{\rm eff}(\Delta\phi)$ at three different parameter values. The label for each curve denotes the corresponding stable synchronization state and the locations of the states are marked by the small squares.

$$\Gamma^{\rm eff}(\Delta\phi)=\frac{1}{2\pi}\int_0^{2\pi}Z(\phi)p(\phi,\Delta\phi)d\phi,\tag{10}$$

where $\Delta\phi$ denotes the phase difference between two oscillators and $p(\phi,\Delta\phi)$ denotes the perturbation due to coupling that depends on the oscillator phases. The sensitivity function, $Z(\phi)\equiv\nabla_X\phi|_{X=X_0(\phi)}$, measures the phase-dependent response of the uncoupled limit cycle (X_0) to the perturbation.

Then, the zeros of $\Gamma_a^{\rm eff}(\Delta\phi)$ correspond to the phase-locked synchronization states and their stabilities are determined from the slope of $\Gamma_a^{\rm eff}(\Delta\phi)$ at the corresponding states: the negative slope means a stable state, and vice versa. Some typical behaviors of $\Gamma_a^{\rm eff}(\Delta\phi)$ at different parameter values are shown in Fig. 6. The three curves in the figure correspond to the three main kinds of the synchronized states: the in-phase (I), antiphase (A), and out-of-phase synchronization (O). Due to the symmetry of Eq. (8), the existence of the in-phase state is trivial. The existence of the antiphase state is also guaranteed due to the periodicity of $\Gamma_a^{\rm eff}(\Delta\phi)$. The out-of-phase state corresponds to the phase-locked state with phase difference between zero and π. The symmetry of Eq. (8) is broken for the out-of-phase states (also for A), but they occur as a pair each of which is symmetric to the other.

From the phase model analysis we observe that different states of synchronization exist depending on the parameter values of μ and Ψ and the parameter space is basically divided into four different regions. Figure 7(a) shows the phase diagram in the polar coordinated plane of (μ,Ψ). The range of μ is given such that the radius of the plane is limited to the μ value for the homoclinic bifurcation. In the figure the blank area corresponds to the in-phase synchronization states (I), the dark gray area to the antiphase states (A), and the

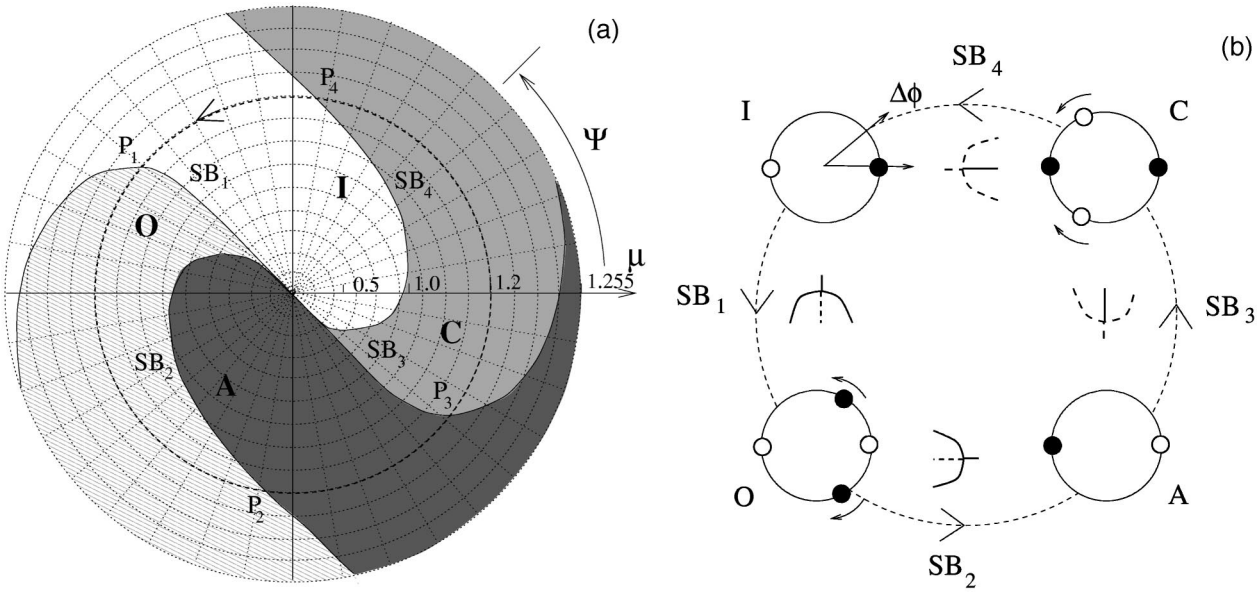

FIG. 7. (a) Phase diagram for the coupled MVP model in the weak-coupling limit. (b) Stability and bifurcation of the synchronization states along the circular path of (a). The insets denote the corresponding symmetry-breaking bifurcations among them.

dashed area to the out-of-phase states (O). The overlap of the I and A areas is denoted by the light gray area (C) in which the in-phase states and the antiphase states coexist. The scale of the radial axis has been nonlinearly transformed to magnify the behavior at larger μ values.

For smaller μ values ($\mu \sim 0.1$, roughly), the diagram shows that the synchronization behavior is qualitatively equivalent to that of the coupled van der Pol oscillators. Namely, the in-phase synchronization is the only stable state in the (purely) diffusive coupling regime. The synchronization states are either of in-phase (I) or antiphase (A), depending on the coupling angle Ψ; the O states live only in a negligibly small area.

For larger μ values, however, synchronization depends not only on Ψ but also on μ. To see the parameter dependence of the behavior, let us set $\mu = 1.2$ and, starting from some value within the I region, say $\Psi = 3\pi/4$, increase Ψ along the circular path as denoted in Fig. 7(a). The in-phase state is the only stable state until it reaches P_1, where the Floquet multiplier of maximum magnitude becomes $+1$. The in-phase state loses stability at this point and two other stable states with broken symmetry (O states) are born. The curve of the symmetry-breaking bifurcations is denoted as SB_1 in the figure. As Ψ is increased, the pair of the out-of-phase states collide with each other and disappear at P_2, where the inverse symmetry-breaking bifurcation (SB_2) occurs, which in turn gives birth to a stable antiphase state (A).

When Ψ is further increased, the in-phase state becomes stable at P_3, while the antiphase state still remains stable. That is, there exists a region where both the in-phase and the antiphase state are stable, as denoted by C in the figure. They coexist until the antiphase state loses its stability at P_4 upon the symmetry-breaking bifurcation with increased Ψ. The bifurcation curves passing through P_3 and P_4 are denoted in Fig. 7(a) as SB_3 and SB_4, respectively. The bifurcations at SB_3 and SB_4 are subcritical in that they are entailed by the presence of two unstable (out-of-phase) states.

To summarize the contrasted behaviors, the phase diagram of Fig. 7(a) shows that the in-phase synchronization is the only stable state for the weak diffusive coupling, especially for $0 \leqslant \Psi \leqslant \pi/2$, which is similar to the behaviors of the coupled van der Pol oscillators. However, this is true only when μ is sufficiently small, that is, when the limit cycle is far from the homoclinic bifurcation. The diagram also shows that the in-phase synchronization may not be the only stable state even in the regime of the diffusive coupling when the limit cycle approaches the homoclinic bifurcation with increased μ. Such a tendency seems to be more outstanding for the case of the position-coupling especially, as one can notice from the presence of the antiphase synchronization as the only stable state at $\Psi \sim 0$ and $\mu \sim 1.255$.

The three synchronization states occur by exchanging their stabilities under the symmetry-breaking bifurcations. The occurrence of the symmetry-breaking bifurcations along the circular path of Fig. 7(a) is schematically depicted in Fig. 7(b). The circles at the four sites represent the variation of the phase difference $\Delta\phi$ and the smaller circles on them denote the synchronization states; the filled small circle denotes the stable state and the empty circle denotes the unstable state. In the insets of the bifurcation diagrams, the branches for in-phase and antiphase states are denoted as straight lines and the emerging pairs of branches for symmetry-breaking O states are denoted as parabolic curves. A solid line denotes a stable branch and a dotted line an unstable branch.

B. Finite coupling strength

When the coupling strength becomes finite, the perturbation of the limit cycle due to coupling can be significant and, consequently, the phase model reduction may not be appropriate for predicting the behavior of the coupled dynamics. Then, one needs to resort to direct numerical methods.

In this subsection, using the techniques of the bifurcation analysis, we examine the synchronization behaviors of the

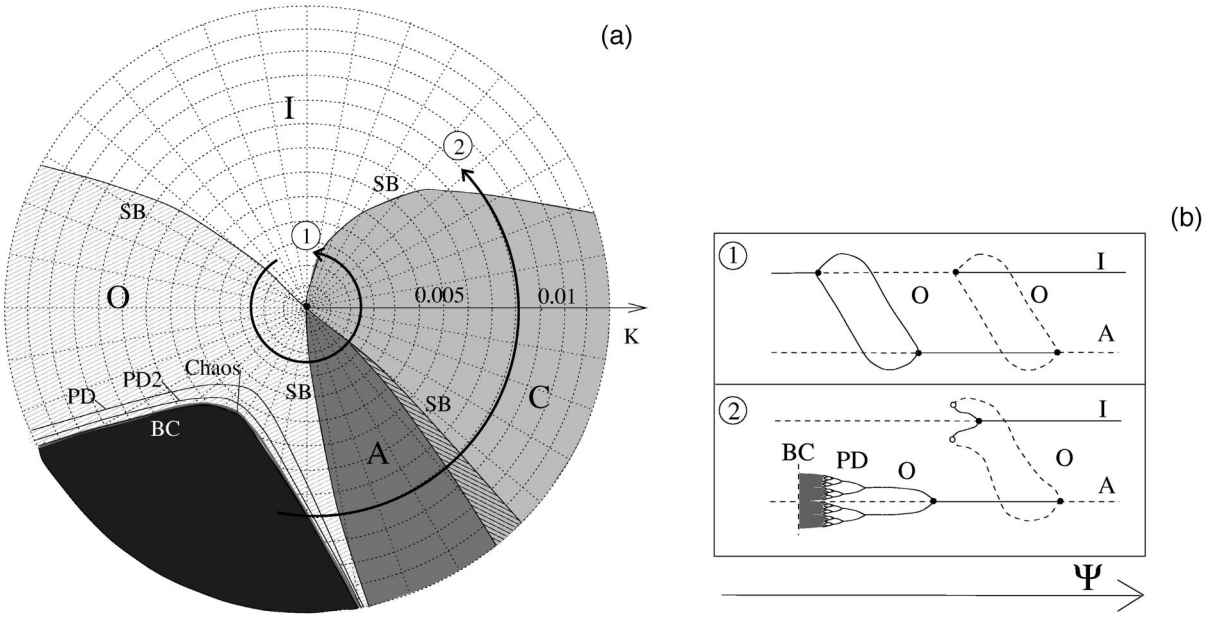

FIG. 8. (a) Phase diagram for the coupled MVP model at $\mu = 1.2$ up to finite coupling strength. (b) Bifurcation diagrams along the paths denoted in (a).

coupled MVP model over a range of the coupling strength, focusing on how the results of the weak-coupling limit in the preceding subsection extend in the regime of the finite coupling strength. Also we obtain the phase diagram for the coupled Morris-Lecar model and compare it with the one for the MVP model to show that the proposed model in a moderate range of the parameters may well display the generic behaviors of the coupled oscillator systems near the homoclinic bifurcation.

Since our primary interest is in the limit cycle oscillations near the homoclinic bifurcation, we fix $\mu = 1.2$ for both the oscillators, which is close to the bifurcation point, and then vary the two coupling parameters, K and Ψ. In particular, our view of interest is limited to the region of the phase space where each oscillator is in a stable oscillatory state; we may call this region ''the region of coupled oscillations.'' Therefore, whenever trajectories leave the region we assume that there are no stable attractors in the region; one mechanism of such disappearance is given via a boundary crisis, the details of which are beyond the present scope.

The resulting phase diagram in the polar coordinated plane (K,Ψ) is shown in Fig. 8(a) in the regime of $K < \sim 0.013$. The occurrence of the boundary crisis is denoted as BC and the region of the parameter space with no attractors in the region of coupled oscillations is colored black in the diagram. Notice that Fig. 7(a) and Fig. 8(a) are drawn in the different parameter planes.

As shown in the weak-coupling limit, there exist three main kinds of synchronization states: the in-phase (I), antiphase (A), and out-of-phase (O) states. As K becomes finite, the region of each state starts to be deformed from the phase model prediction, which is manifested by the deflection of the bifurcation lines that depend on K. Besides the symmetry-breaking bifurcation described previously, the states may also undergo other bifurcations such as period doubling that cannot be predicted from the phase model description either.

Typical behaviors of the transitions and their coexistences are depicted in Fig. 8(b) along the Ψ paths with two different K values: the two paths are labeled as shown in Fig. 8(a). The branches in the diagrams are drawn using the same conventions as in Fig. 7(b). In each subset the upper horizontal line denotes the in-phase state branch (I) and the lower line denotes the antiphase state branch (A). Note that the diagram depicted for path 1 of smaller K coincides with the behavior observed in the case of the weak-coupling limit [Fig. 7(b)].

Path 2 of larger K includes the period-doubling cascades of O states. Namely, an A state undergoes the symmetry-breaking bifurcation, resulting in two symmetric branches of stable O states. As Ψ is decreased, the O states at each branch undergo the period-doubling cascades and these cascades lead to the onset of chaos and are symmetric to each other as well. As Ψ is further decreased, two chaotic attractors merge to form a single chaotic attractor, which then restores the symmetry. This symmetric chaotic attractor eventually disappears via a boundary crisis and the trajectory leaves the region of coupled oscillations. The period-doubling cascades of O states also occur at the other side of the BC region.

In Fig. 8(b), from the diagram corresponding to path 2, one may also notice that the saddle-node bifurcation of the out-of-phase states provides an additional source for the birth of a pair of the O states, which can be viewed as the connection of a stable and an unstable branch of the O state that originate from different states, I and A, respectively. This saddle-node bifurcation is not observed in the weak-coupling limit [Fig. 7(a)] even though they can occur in the phase model description; the saddle-node bifurcation occurs at the tangency of Γ_a^{eff} in Fig. 6. The region of these O states is denoted in Fig. 8(a) as the dark dashed area.

For a comparison with the neuronal model, the phase diagram for the coupled Morris-Lecar model is shown in Fig. 9. For this model the homoclinic bifurcation takes place at I_{dc}

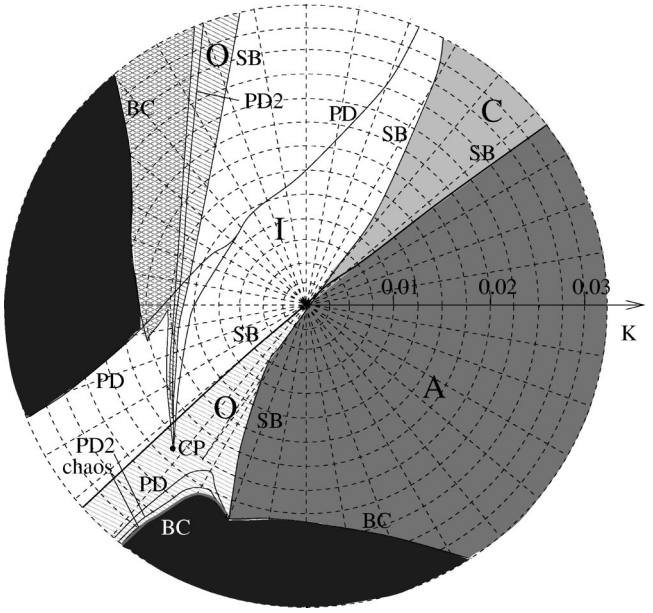

FIG. 9. Phase diagram for the coupled Morris-Lecar model at $I_{dc}=0.0750$.

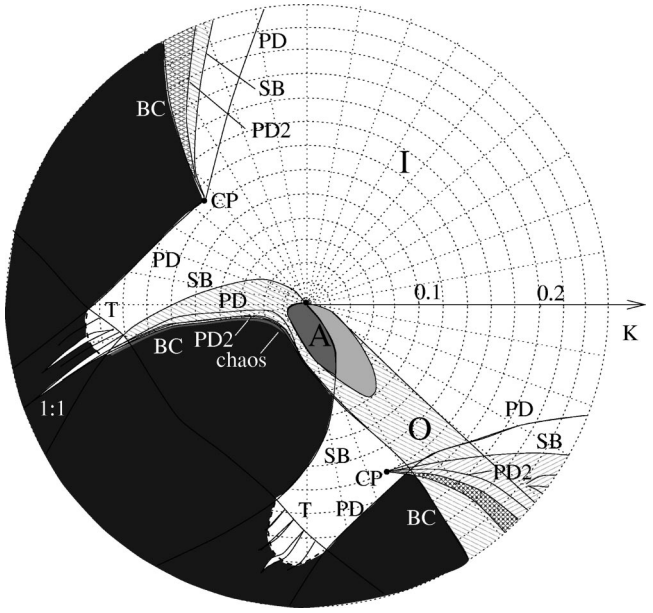

FIG. 10. Phase diagram for the coupled MVP model at $\mu=1.0$ up to stronger coupling strength.

≈ 0.0729 and the diagram has been obtained at $I_{dc}=0.0750$, close to the homoclinic bifurcation. The broader region of chaos following the period-doubling cascades is denoted by the hatched area in the figure.

The organization of the various states for the Morris-Lecar model is not precisely the same as for the MVP model, which should vary depending on specific models. It is also likely that the range of the parameters such as I_{dc} and K has not been chosen to best show a better coincidence. Nevertheless, the features in the regime of the weak-coupling strength are essentially the same for both models in terms of the existence of the bifurcations and the pattern of their occurrences. More importantly, the diagrams show that both systems have stable dephased synchronization in a wide range of the diffusive coupling regime, which has been the primary interest of the present examination. Figure 9 also shows the existence of a cusp point (CP) to which many regions for different states merge. The cusp point is not peculiar to the Morris-Lecar model, as such examples will also show for the MVP model at different parameter regimes (see the following subsection).

C. Strong coupling with an intermediate μ

So far we have emphasized a contrast between the behaviors of the coupled oscillators in two distinctive regimes in the aspect of the closeness to the homoclinic bifurcation, that is, the coupled van der Pol–type oscillators and the coupled oscillators near the homoclinic bifurcation. In this subsection we examine the behavior of the coupled MVP model in an intermediate regime between those distinctive regimes, which we may consider to be provided by setting the parameter at $\mu=1.0$. In particular, the case of the stronger coupling strength is considered since it turns out that the weak coupling results in rather trivial behaviors that have been already observed in Sec. V A. The phase diagram in this regime of the parameters is shown in Fig. 10, which demonstrates a variety of complex behaviors.

The in-phase synchronization states, in addition to the symmetry-breaking bifurcation described previously, may undergo two more kinds of bifurcations: the period-doubling and the torus bifurcation. The period-doubling either gives birth to a stable period-doubled in-phase state, or to none of the stable attractors. In the former case, the period-doubled in-phase state undergoes the symmetry-breaking bifurcation, which in turn gives birth to a pair of out-of-phase states. These out-of-phase states undergo a cascade of period-doublings, leading to chaos in the same way as observed for the O states in Fig. 8. Two such cases are shown in Fig. 10 to the northwest and the southeast directions.

The latter case of the period-doubling bifurcation entailing no attractors implies the occurrence of the boundary crisis with an attractor outside the region of coupled oscillations. Therefore, the trajectory suddenly disappears from the region of coupled oscillation. The regime of the parameters for this case is denoted by the black area in the diagram. The period-doubling bifurcations of the in-phase states resulting in these two cases also occur for the Morris-Lecar model, as can be found in Fig. 9.

The torus bifurcation of the in-phase states occurs when a complex conjugate pair of the Floquet multipliers leaves the unit circle in the complex plane. The bifurcating torus is observed to retain the symmetry of Eq. (8). The flows on the torus are those for the coupled systems with two competing frequencies. Below the curve for the torus bifurcation (T) in Fig. 8(a), note the existence of the familiar resonant tongues corresponding to the frequency-locked states with rational rotation numbers. The most prominent among them is the tongue of the one-to-one locking, which is denoted in the diagram. Notice also that the tongues can persist even in the absence of the stable torus nearby in the parameter space. The torus disappears via a boundary crisis. The torus bifurcation also occurs for the Morris-Lecar model even though such a case is not indicated in Fig. 9; it is observed to occur at a stronger coupling strength, $K\sim 0.15$.

A special notice is on the existence of the cusp points in the northwest and the southeast directions in Fig. 10 (CP in the diagram), to which all the regions of the period-doubling merge to form a common boundary; they are observed to be the cusp points within the numerical resolution. Such a location implies that the codimension of the bifurcation would be infinite. Interestingly, the cusp point also exists in the Morris-Lecar model as shown in Fig. 9. Possible questions such as its genericity and the unfolding prompt further investigations.

Again, the global organization pattern of the phase diagram in Fig. 10 is not quite the same as for the Morris-Lecar model in Fig. 9. However, as we have already noticed in this subsection, the coincidences between the local behaviors in the two models are striking. Therefore, in this sense of similarities, it seems that the proposed MVP model represents well the Morris-Lecar model over a wider range of the parameter space not just restricted to the neighbors of the homoclinic bifurcation with a rather weak-coupling strength. We presume that this representation can be also approriate for other models having the structure of Fig. 1.

VI. CONCLUSIONS

Synchronization between coupled oscillations has been shown to display distinctive behaviors as the limit cycle oscillation approaches the homoclinic bifurcation. In this paper, a generic physical model for studying such behaviors has been proposed using the modified van der Pol equation. A general form of coupling has been also considered by introducing the vector coupling between the variables of the two-dimensional oscillators.

The homoclinic bifurcation implies the presence of a saddle near the limit cycle. The dephasing mechanism of the synchronized oscillations in the vicinity of the saddle has been analyzed both qualitatively and quantitatively in the weak-coupling limit. The dephasing rate measured by the linear rate Q is shown to increase dramatically as the limit cycle approaches the homoclinic bifurcation.

The synchronization behaviors of the coupled MVP oscillators have been examined over a wide range of the coupling parameters. In the weak-coupling limit the phase model reduction method has been used to show the existence of the main synchronization states and to identify the transitions among them through the symmetry-breaking bifurcations. For the finite coupling strength we have resorted to the direct numerical calculations using the techniques of the bifurcation analysis, which has revealed the extended behaviors that cannot be predictable from the phase model description. In both cases the phase diagrams have been obtained and it has been shown that the in-phase synchronization may not be the only stable state in the regime of the diffusive coupling as the limit cycle approaches the homoclinic bifurcation.

The intermediate regime has also been examined where the coupled oscillators are in between the two distinctive regimes of the van der Pol–type oscillators and the oscillators near the homoclinic bifurcation. A variety of complex behaviors, including the period-doubling and the torus bifurcations, the mode-locking tongues, and chaos arises in this regime as the coupling strength becomes larger, for which the phase diagram has also been constructed.

The phase diagrams for the MVP model have been compared with the one for the Morris-Lecar model, which is only an example of the neuronal models that have provided motivations for the present study. The comparison leads to a reasonable conclusion that the synchronization behaviors observed in the MVP model should be generic for the systems of coupled oscillators near the homoclinic bifurcation. The close coincidences between the local behaviors of the models have also been observed over a wider range of the parameter space, which is not restricted only to the neighbors of the homoclinic bifurcation with a rather weak-coupling strength.

ACKNOWLEDGMENTS

The authors would like to thank Y. Kuramoto, C. Kurrer, S. Kim, and A. Neiman for useful discussions. D.P. was supported by the STEPI of Korea through the Korea-Russia scientist exchange program during his stay at the Physics Department of Chungbuk National University. S.K.H. was supported by the Korea Research Foundation in the program year of 1988. H.K. is thankful for the support of the ICTP for his visit, during which the part of the present work was done and also to the Brain Research Foundation of the Ministry of Science and Technology.

[1] Y. Kuramoto, *Chemical Oscillations, Waves, and Turbulence* (Springer-Verlag, Tokyo, 1984).

[2] A. T. Winfree, *The Geometry of Biological Time* (Springer, New York, 1980).

[3] C. M. Gray, P. König, A. K. Engel, and W. Singer, Nature (London) **338**, 334 (1989).

[4] R. Eckhorn, R. Bauer, W. Jordan, M. Brosch, W. Kruse, M. Munk, and H. J. Reitboeck, Biol. Cybern. **60**, 121 (1988).

[5] C. von der Malsburg and C. Schneider, Biol. Cybern. **54**, 29 (1986).

[6] J. Guckenheimer and P. Holmes, *Nonlinear Oscillations, Dynamical Systems, and Bifurcations of Vector Fields* (Springer-Verlag, New York, 1983).

[7] R. H. Rand and P. J Holmes, Int. J. Nonlinear Mech. **15**, 387 (1980).

[8] D. G. Aronson, E. J. Doedel, and H. G. Othmer, Physica D **25**, 20 (1987).

[9] A. Sherman and J. Rinzel, Proc. Natl. Acad. Sci. USA **89**, 2471 (1992).

[10] S. K. Han, C. Kurrer, and Y. Kuramoto, Phys. Rev. Lett. **75**, 3190 (1995).

[11] S. K. Han, C. Kurrer, and Y. Kuramoto, Int. J. Bifurcation Chaos **7**, 869 (1997).

[12] C. Morris and H. Lecar, Biophys. J. **35**, 193 (1981).

[13] J. Hindmarsh and M. Rose, Proc. R. Soc. London, Ser. B **221**, 87 (1984).

[14] D. Hansel, G. Mato, and C. Meunier, Europhys. Lett. **23**, 367 (1993).